Experimental and numerical study on crack initiation under fretting fatigue loading

M. Luke *, M. Burdack, S. Moroz, I. Varfolomeev

Fraunhofer Institute for Mechanics of Materials IWM, Wöhlerstraße 11, 79108 Freiburg, Germany

*corresponding author, phone +49 761 5142 338

E-mail addresses:

michael.luke@iwm.fraunhofer.de, michael.burdack@iwm.fraunhofer.de,

sergii.moroz@iwm.fraunhofer.de; igor.varfolomeev@iwm.fraunhofer.de

Abstract

Press-fitted railway axles and wheels are subjected to fretting fatigue loading with a potential hazard of crack initiation in press fits. Typically, the resistance against crack initiation and propagation in press fits is investigated in full-scale tests, which procedure is both costly and time consuming. In this context, combined experimental and numerical approaches are of increasing practical importance, as these may reduce the experimental effort and, moreover, provide a basis for the transferability of experimental results to different axle geometries and materials. This study aims at evaluating stress-strain conditions under which fretting fatigue crack initiation is likely to occur. Experiments on small-scale specimens under varying fretting fatigue load parameters and their finite-element modelling to characterize the resulting stress-strain fields are performed. Subsequently, different multiaxial fatigue parameters are applied to predict crack initiation under fretting fatigue conditions.

Keywords: fretting fatigue; crack initiation; multiaxial fatigue damage parameter

Introduction

Fretting fatigue is a complex phenomenon which has been investigated in many respects by different researches, e.g. [1-7]. Material behaviour under fretting fatigue is influenced by various factors, e.g. material pairing, contact area geometry, multiaxial stress state within the contact zone, surface

roughness, environmental effects, coefficient of friction, loading velocity. The fatigue life of railway axles can be limited by crack initiation in press fitting locations, in particular within the contact zone between the axle and the wheel. Both the service experience and laboratory tests reveal that, under certain conditions, circumferential cracks can initiate in press fits subjected to rotary bending, caused by small relative movements of friction surfaces being in contact. The risk of axle failure can then arise if such cracks propagate in the radial direction. Currently, the resistance of press-fitted railway axles and wheels against crack initiation and crack propagation as well as technical developments subjected to the improvement of the fretting fatigue crack resistance are investigated mainly in full-scale axle tests, see Fig. 1 [8].

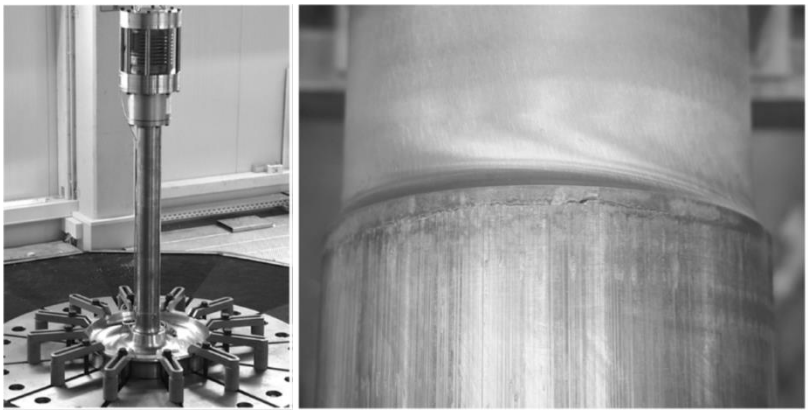

Fig. 1: Example of a test rig for fatigue strength assessment of axles in press fits (left) and fatigue cracks in a press fit (right). Taken from [8].

However, such tests are time consuming and expensive. Furthermore, results gained from a particular test series are not directly transferable to other combinations of the axle design and material. Therefore, combined experimental and numerical assessment procedures helping to reduce the experimental effort are essential from the practical point of view. The aim of this study performed within the framework of the research project EURAXLES [9] is to contribute to the development of a methodology by which means the number of expensive full-scale axle tests can be reduced or replaced by small-scale specimen testing accompanied by numerical analyses. For this purpose, a series of small-scale specimen tests is performed under fretting fatigue conditions using a specially designed test set-up. The load parameters, such as the stress amplitude, contact load and relative slip between the contact surfaces, were varied or selected to achieve conditions relevant for axles in service.

Additionally, numerical analyses of the test specimens are performed to estimate the respective stress-strain fields and evaluate a potential applicability of multiaxial fatigue parameters for predicting material damage under fretting fatigue conditions. Note that issues of the fatigue crack propagation in press fits are out of scope of this study.

1. Experimental Set-Up

To experimentally simulate loading scenarios which are relevant for fretting fatigue initiation due to relative movements within the contact zone of an axle-wheel press fit connection, a test concept [1, 2] schematically shown in Fig. 2 (left) was adopted in this study. During a test, cyclic axial loading with a constant stress amplitude (or a maximum stress σ_{appl}) is applied to the specimen end by means of a standard testing machine (here resonant testing machine). The transverse contact load Q is applied and controlled by an independent hydraulic system via contact pads which clamp the specimen from two opposite sides. Thus, definite load combinations can be introduced which lead to a relative slip δ between the specimen and the pads within the contact zone. The resulting displacement should be small with respect to the total contact length in order to evoke fretting fatigue conditions [7]. In particular, the range of the contact slip realized in this study varied within some $5 - 20$ µm, while the width of the contact zone was about $l_c = 1.7$ mm. To implement the above test concept, the set-up shown in Fig. 2 (right) was designed and manufactured. It consists of a horizontally positioned hydraulic loading system transmitting the lateral pressure forces symmetrically through two pads to the specimen, whereas the latter is fixed in a resonant testing machine and loaded in the vertical direction.

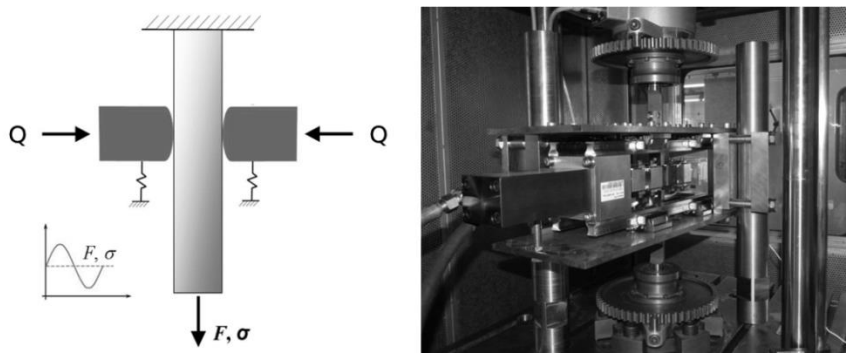

Fig. 2: Schematic representation of the fretting fatigue test concept [1, 2] (left) and test fixture adopted in this study (right).

In the tests, two specimen geometries were used as shown in Fig. 3. Both specimens have a width of $w = 6$ mm, whereas the uniform lengths were chosen to be $l_s = 21$ mm (specimen #1) and $l_s = 100$ mm (specimen #2), respectively. When increasing the specimen length, the overall longitudinal displacement and the resulting contact slip were also increased.

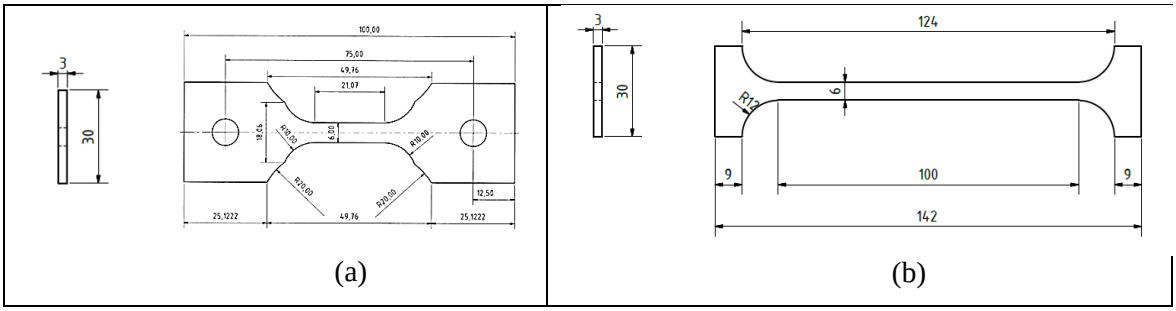

Fig. 3: Specimen geometries used in fretting fatigue tests: a) specimen #1; b) specimen #2.

Two pad geometries shown in Fig. 4 were used in the tests. The overall pad width was $w_p = 12$ mm, while the contact side was machined as either a continuously round surface with a radius of $r = 50.8$ mm or being additionally flattened over a length of $l_c = 1.7$ mm (type B). In the latter case, the resulting nominal contact area estimated at $Q = 0$ kN was $w \times l_c = 6 \times 1.7 = 10.2$ mm^2. In contrast, the type A pad produces a narrow contact zone with an indefinite width, thus leading to less reproducible test results. As a consequence, no fretting fatigue cracks were observed when using type A pads and applying the same load parameters as in the tests with the flattened pad geometry. Consequently, the test results reported in Section 2 refer to the specimen geometries #1 and #2 in combination with the type B pad.

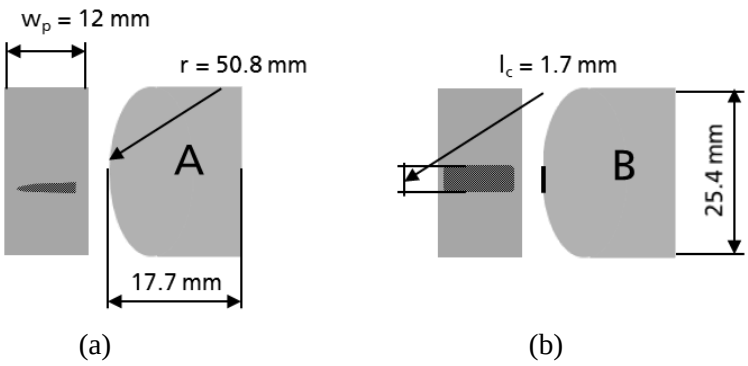

Fig. 4: Pad geometries employed in tests with a schematic of the surface contact:
a) round contact surface (type A); b) flattened contact surface (type B).

All fretting fatigue tests were performed using the material pairing EA4T (25CrMo4, quenched and tempered, see DIN EN 13261) for the specimens and ER8 for the pads (machined from a railway

wheel hub, see DIN EN 13262), at room temperature and under laboratory conditions. Due to using a resonant testing machine, all tests were conducted at load frequencies ranging between 120 and 140 Hz which is by a factor of about 5 to 10 higher than the load frequency in relevant applications. Possible load frequency (or load rate) effects were not investigated in the present study.

2. Test results

Table 1 summarizes the specimen geometry data, load parameters and test results for a series of tests using the flattened pad geometry. A total number of 16 tests were performed at a stress ratio of $R = 0.1$. All specimens were loaded to a pre-defined number of cycles, whereas none of the specimens failed during the test. Since the contact area was offset from the specimen center by 10 mm, most of the specimens were tested twice applying the transverse load to a different specimen zone in the second test. After having reached the pre-defined number of cycles, the specimens were removed from the testing machine and examined in a light microscope (LM) to detect fretting fatigue cracks. Note that cracks could only be detected at specimen surfaces which have been polished before testing and additionally cleaned using an oxide polishing suspension (Eposil, 1 µm diamond suspension) and a polishing felt, to remove abrasion and corrosion debris before performing the light microscopic analyses.

Specimen no.	Specimen geometry (Fig. 3)		Contact zone	Load parameters		Load cycles	Crack initiation
	#	uniform length l_s, mm		σ_{appl}, MPa	Q, kN		
9	1	21	1	350	3	5×10^6	•
11	1	21	1	350	3	10^6	•
			2	330	1.5	10^6	•
12	1	21	1	270	1.5	10^6	•
			2	350	1.5	10^6	•
13	1	21	1	200	1.5	10^6	–
			2	250	1.5	10^6	–
14	1	21	1	300	1.5	10^6	•
			2	270	1.5	10^6	•
15	1	21	1	350	1.5	2×10^5	•
41	2	100	1	250	1.5	10^6	•
			2	200	1.5	10^6	–
42	2	100	1	350	1.5	10^6	•
			2	300	1.5	10^6	•
43	2	100	1	350	1.5	10^6	•
			2	200	1.5	10^6	–

Table 1: Overview of fretting fatigue tests using flattened pads.

By trying different geometries of specimens and pads, fretting fatigue cracks were found to initiate under following combinations of the specimen geometry and loading conditions:

1. Overall specimen length $L = 100$ mm, uniform specimen length $l_s = 21$ mm

- $N = 10^6$ cycles at $Q = 1.5$ kN and $\sigma_{appl} = 270 - 350$ MPa
- $N = 2 \cdot 10^5$ cycles at $Q = 1.5$ kN and $\sigma_{appl} = 350$ MPa
- $N = 10^6$ to $N = 5 \cdot 10^6$ cycles at $Q = 3$ kN and $\sigma_{appl} = 350$ MPa

2. Overall specimen length $L = 142$ mm, uniform specimen length $l_s = 100$ mm

- $N = 10^6$ cycles at $Q = 1.5$ kN and $\sigma_{appl} = 250 - 350$ MPa (with an increased uniform specimen length)

The load parameters were selected to achieve conditions representative for wheel seats in operation or under test conditions. For instance, the transverse load of $Q = 1.5$ kN acting over a contact area of $w \times l_c = 6 \times 1.7 = 10.2$ mm^2 produces the nominal contact stress of about 150 MPa. For comparison, contact stresses estimated in press fits of full-scale axles tested in [8, 9] on the so-called "Minden type" axle test rig were in the range of 60-150 MPa with the lower and upper stress ranges corresponding to the mean and maximum values of the interference, respectively. The above stresses refer to a location of 2-5 mm from the press fit border where fretting fatigue cracks were observed in the respective tests [8, 9].

Fig. 5 and Fig. 6 show characteristic crack patterns detected by means of the LM analysis. The respective cracks were initiated on the specimen surface along the edge of the contact zone within an area subjected to the maximum contact slip (cf. Fig. 13 and Fig. 14). The cracks are orientated transverse to the tension load direction and have lengths varying from approximately 20 µm to 400 µm, whereas the larger cracks likely result due to the growth and coalescence of multiple cracks. Typical positions and orientation of the fretting fatigue crack is schematically shown in Fig. 7.

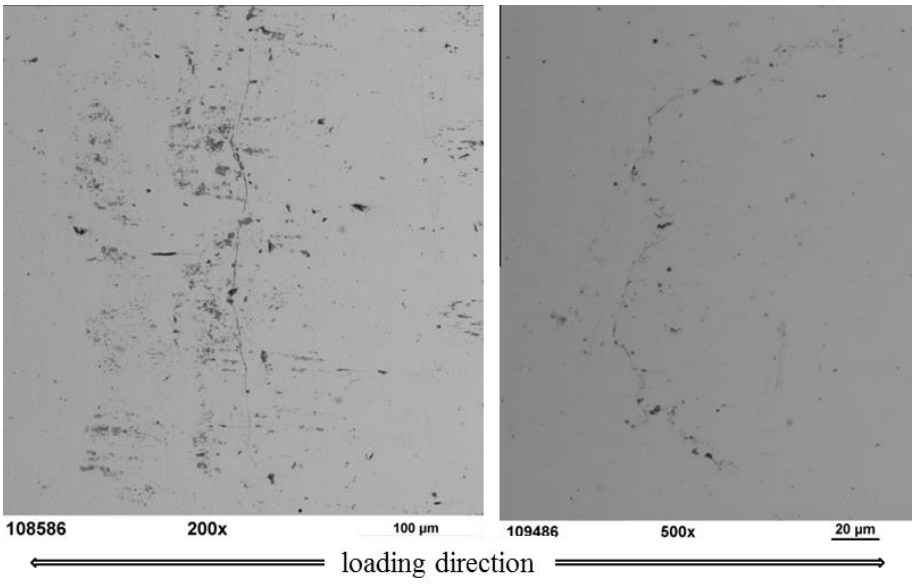

Fig. 5: Examples of fretting fatigue cracks detected via LM analyses. Left: specimen no. 9, $\sigma_{appl} = 350$ MPa, $Q = 3$ kN, $N = 5 \cdot 10^6$ cycles; right: specimen no. 11, $\sigma_{appl} = 330$ MPa, $Q = 3$ kN, $N = 10^6$ cycles.

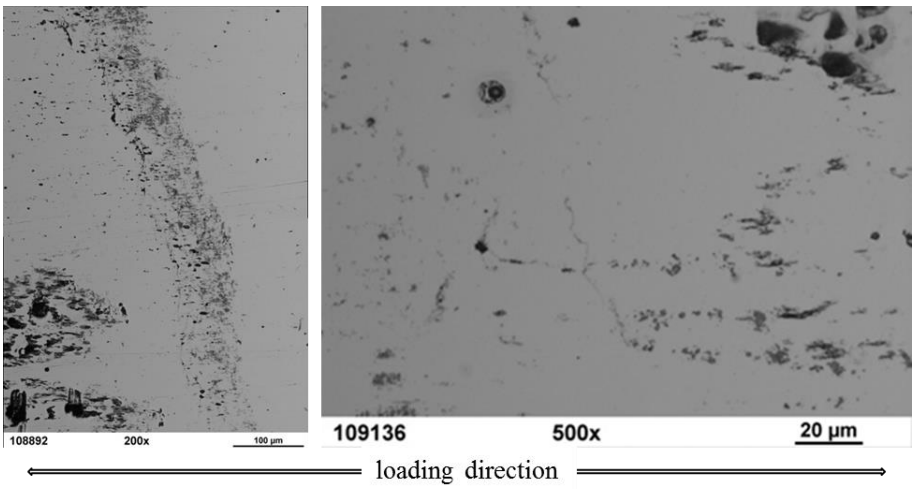

Fig. 6: Examples of fretting fatigue cracks detected via LM analyses. Left: specimen no. 12, $\sigma_{appl} = 350$ MPa, $Q = 1.5$ kN, $N = 10^6$ cycles; right: specimen no. 41, $\sigma_{app}l = 250$ MPa, $Q = 1.5$ kN, $N = 10^6$ cycles.

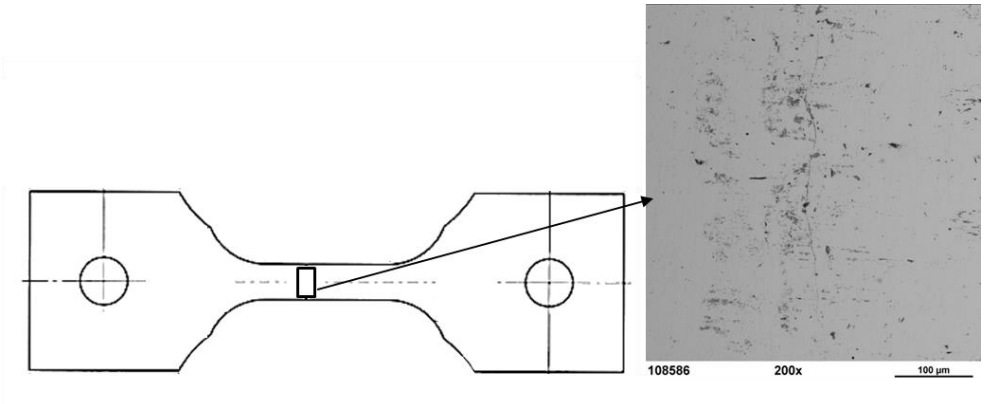

Fig. 7: Typical position and orientation of fretting fatigue cracks.

In Fig. 8, the pressure marks of the contact pads on two different specimens are depicted. Despite of the same specimen and pads geometries used in the respective tests, the pressure mark geometries differ both at the opposite specimen surfaces and for different specimens. This indicates an inherent difficulty of fretting fatigue testing, as most of the influencing parameters, such as the contact area, contact stresses, surface roughness and coefficient of friction, can be controlled to a limited extent.

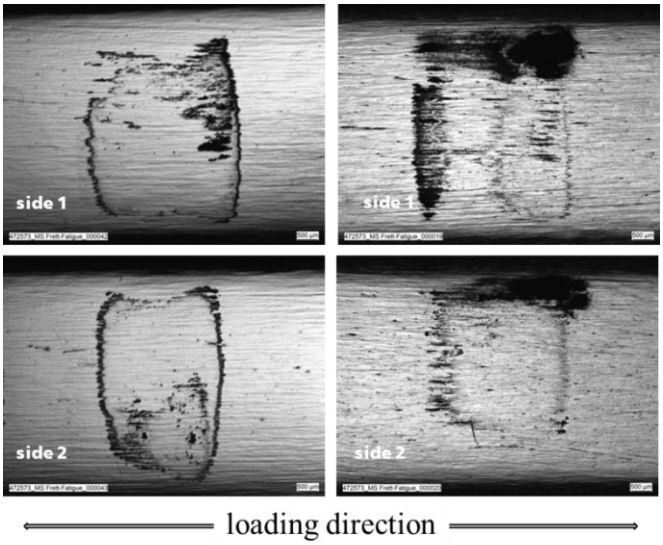

Fig. 8: Pressure marks of contact pads on specimens after fretting fatigue tests. Left: specimen no. 17, $\sigma_{appl} = 330$ MPa, $Q = 3$ kN, $N = 10^6$ cycles; right: specimen no. 41, $\sigma_{appl} = 250$ MPa, $Q = 1.5$ kN, $N = 10^6$ cycles.

All test results summarized in Table 1 were obtained using flattened pads, see Fig. 3. Although not reported here, some preliminary tests were also performed using pads having a continuously round surface with a radius of $r = 50.8$ mm, thus producing a narrow contact zone with an indefinite width. In those tests, no fretting fatigue cracks were observed when applying the same nominal tensile stresses σ_{appl} and transverse loads Q as in the tests with the flattened pads.

3. Numerical Analyses

3.1 Numerical Modelling of Tests

To evaluate the results of fretting fatigue tests, a series of finite-element analyses (FEA) were performed using the FE code ABAQUS, Version 6.12. Fig. 9a shows a two-dimensional FE model of the specimen #1 (Fig. 3a) and the flattened contact pad (Fig. 4b). The specimen length in the model is limited to 50 mm, corresponding to the length of the deformable specimen part, cf. Fig. 3a. The

numerical analyses were performed assuming plane strain conditions which are a rough approximation to a more complex stress field, as can be deduced from Fig. 9. The same holds for the symmetry condition imposed on the FE model with respect to the middle plane of the specimen (plane $y = 0$). The left end of the specimen in the model is fixed in the axial direction (x axis), while an alternating tensile stress with the maximum value of σ_{appl} and the stress ratio of $R = 0.1$ is applied to the right end. The specimen thickness and width are 3 mm and 6 mm, respectively, according to the real dimensions. Rectangular elements with the length of 10 µm and the height of 7.5 µm are used within and near the contact zone (Fig. 9b). Throughout the model, four-node quadrilateral, isoparametric, fully integrated elements are employed. The contact interaction is modelled assuming a constant coefficient of friction of $COF = 0.6$.

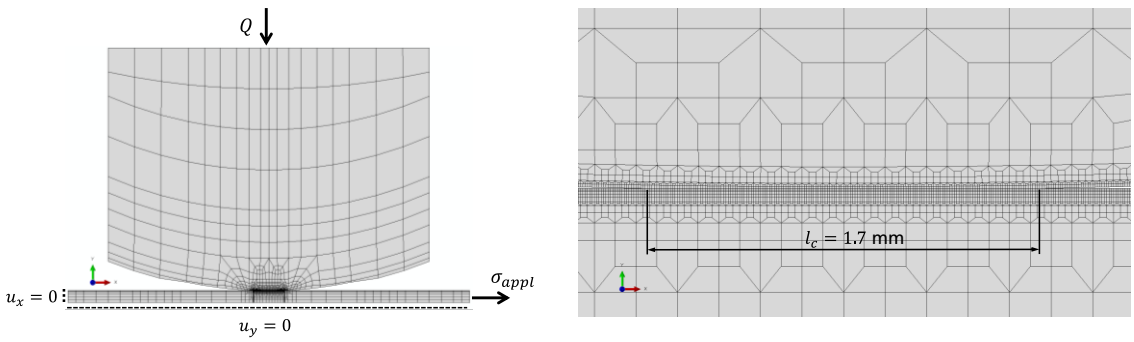

(a) (b)

Fig. 9: FE model of the specimen and pad assembly (a); detail of the contact zone with the definition of the initial contact length (b).

The initial contact zone length, l_c, corresponding to a zero value of the transverse load is indicated in Fig. 9b. When increasing Q and applying the tensile load, the size of the contact zone and the stress distribution within the contact area change in a non-linear manner, so that the estimated location of crack initiation depends on the combination of Q, σ_{appl} and COF values. Based on results of stress-strain calculations, some elements in the FE model were identified as potential sites of crack initiation. Three of those elements representative for evaluating the results at $Q = 3$ kN are marked in Fig. 10a. In the non-loaded state, these elements are positioned 50 to 80 µm outside the initial contact zone. As shown in Fig. 10b, upon applying the normal load $Q = 3$ kN and an axial stress $\sigma_{appl} = 350$ MPa, the respective elements become located within or rather at the border of the contact area and the respective plastic zone.

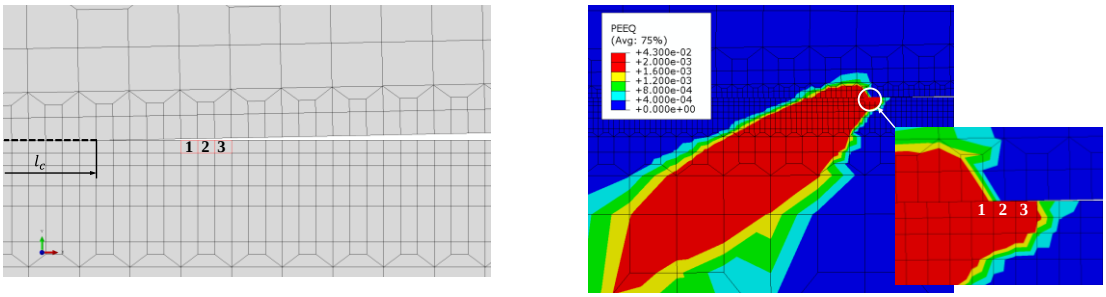

Fig. 10: Location of three elements used in the stress evaluation with respect to (a) the initial contact zone and (b) the plastic zone at maximum load.

To account for plastic deformations of the specimen due to contact, the cyclic plasticity model according to Lemaitre and Chaboche [10] implemented in ABAQUS was employed. Thereby, a combined isotropic-kinematic hardening rule was assumed with the respective model parameters adjusted to fit cyclic stress-strain data determined for the material EA4T in strain controlled incremental step tests. Fig. 11 shows the measured stress-strain hysteresis loops, as well as their approximation by the selected material model. Due to the lack of elastic-plastic properties for the ER8 material, the pad was modelled using the same stress-strain curves as for the specimen. Comparative calculations performed assuming elastic-plastic behaviour of the specimen and elastic behaviour of the pad revealed a negligible effect of plastic deformations of the pad on the stress-strain field in the specimen (cf. Fig. 12c and d).

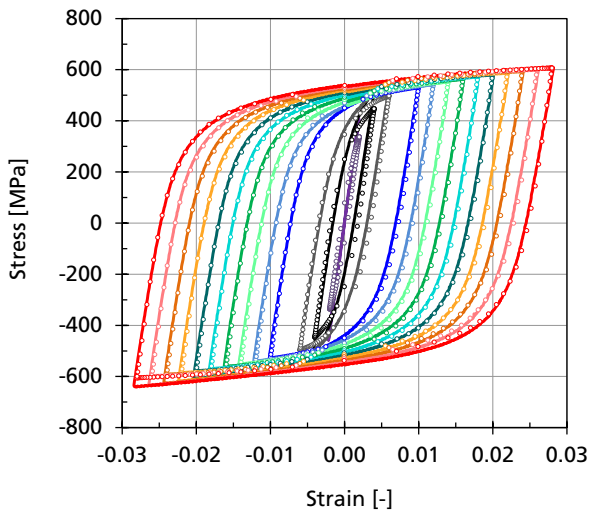

Fig. 11: Stabilized stress-strain hysteresis loops (curves) at various strain amplitudes and their approximation by the Lemaitre-Chaboche model (symbols). Material EA4T.

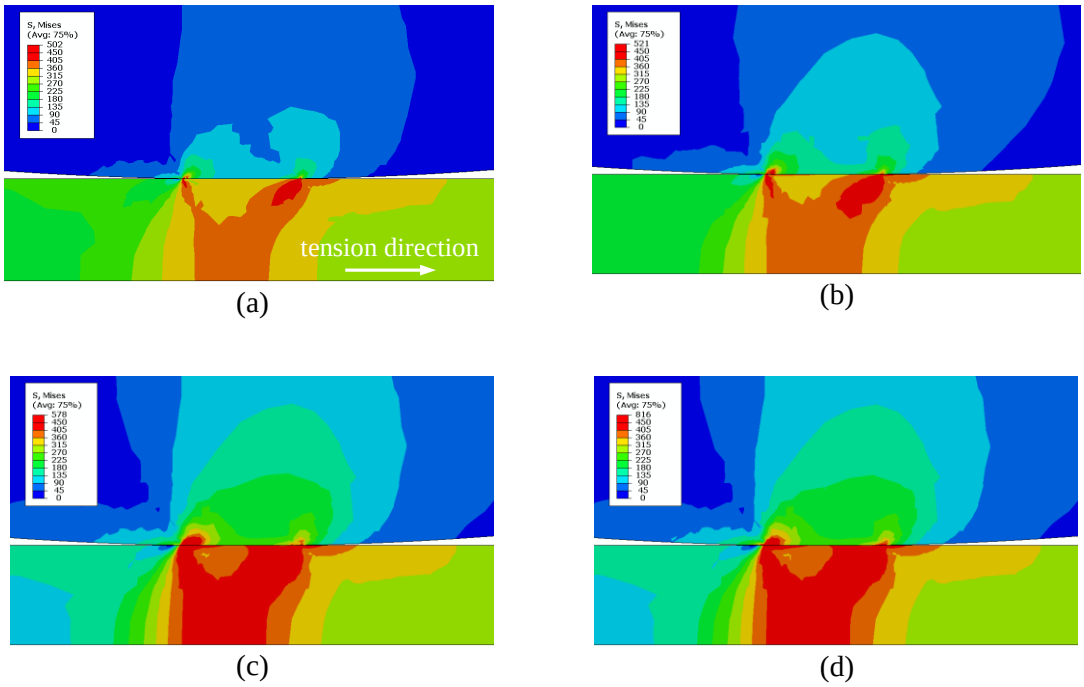

Fig. 12: Equivalent von Mises stress at the maximum applied stress $\sigma_{appl} = 350$ MPa and different normal load: a) $Q = 1.5$ kN; b) Q=2 kN; c) $Q = 3$ kN; d) $Q = 3$ kN, elastic material for the pad.

Fig. 12 compares the patterns of the equivalent von Mises stress calculated at a maximum tensile stress of 350 MPa and different values of the transverse load of Q = 1.5 kN (a), Q = 2 kN (b) and Q = 3 kN (c). Note that the cyclic yield strength for the material EA4T was estimated to be about 450 MPa. Accordingly, the peak values of the equivalent stress are achieved at the specimen surface, close to the border of the contact zone. In all cases, the stress maximum is located at the right contact border (tension direction), whereas the plastic zone progressively develops at both sides of the contact zone with increasing the normal load.

The corresponding relative slips of the nodes within the actual contact zones are shown in Fig. 13 and Fig. 14 for the specimen geometries #1 and #2, respectively. In particular, Fig. 13 suggests that an increase of the transverse force considerably decreases the slip magnitude and changes the shape of the distribution curve. For instance, a shallow gradient of the contact slip curve is determined in the case of $Q = 1.5$ kN, which indicates that both fretting and wear mechanisms may be present at a low contact pressure. In contrast, at $Q = 3$ kN, the relative movement of the contact surfaces is concentrated at an outer border of the contact area, thus promoting crack initiation at that specific location. Such loading conditions are in line with those achieved in axle press-fits and observations

made in full-scale axles tests where fretting fatigue cracks are initiated at a certain distance from the press fit border, see e.g. [8, 9].

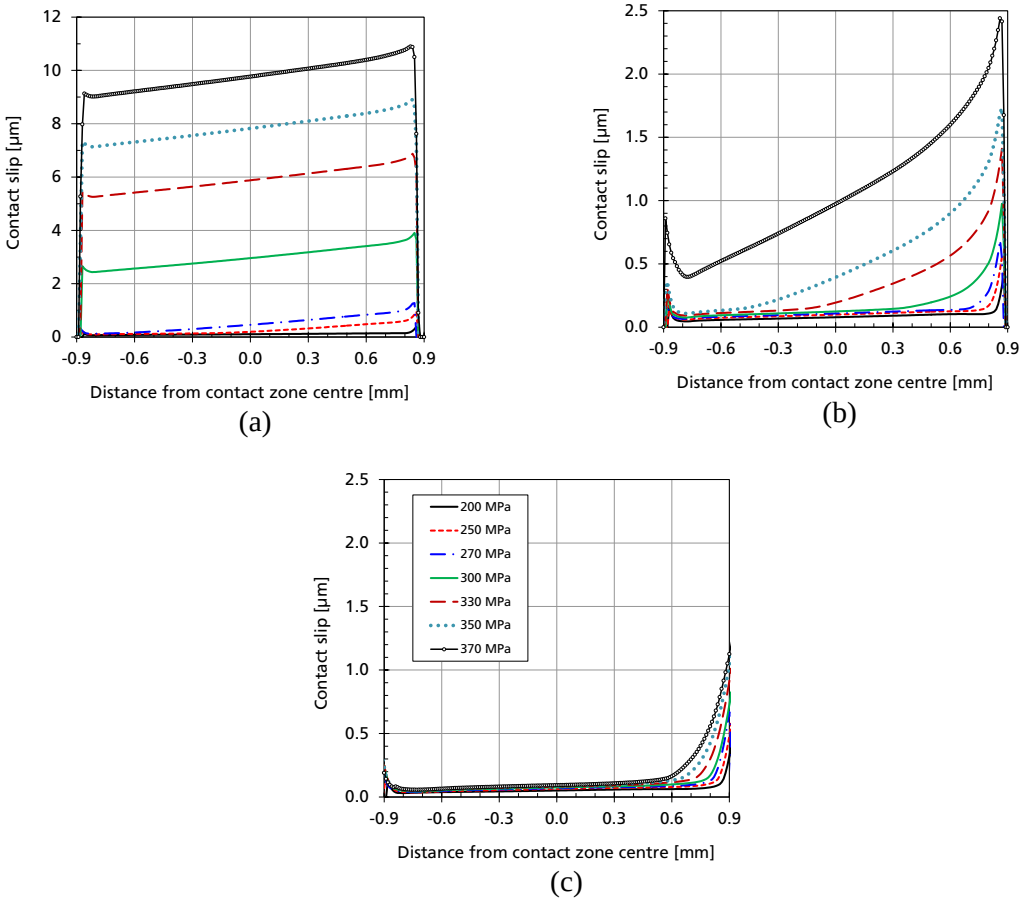

Fig. 13: Contact slip at different maximum applied stress (values in the caption) and transverse load:

a) $Q = 1.5$ kN; b) $Q = 2$ kN; c) $Q = 3$ kN. Specimen geometry #1.

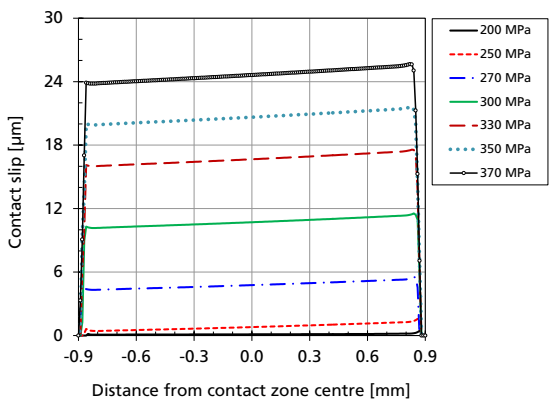

Fig. 14: Contact slip at different maximum applied stress and transverse load Q=1.5 kN. Specimen geometry #2.

When comparing the results in Fig. 13a and Fig. 14, both corresponding to $Q = 1.5$ kN, a similarity of the slip patterns can be concluded for the specimen geometries #1 and #2. However, the absolute slip values for the longer specimen (#2) are about twice to 4 times higher, as compared to the specimen #1 at the same tension stress amplitudes. These results correlate with the experimental findings in Section 2 showing that the stress at crack initiation reduces from 270 MPa for the shorter specimen to 250 MPa for the longer specimen.

3.2 Fatigue Damage Parameters

Evaluation of the conditions for crack initiation under fretting fatigue in terms of the nominal tension stress amplitude, contact stress (both as measures of the external load) and/or contact slip is rather uncertain due to a complex interaction of the above parameters. As an alternative approach, fatigue damage parameters can be employed to characterize the multiaxial stress state and, moreover, to account for non-proportional variations of stresses and strains within and near the contact zone, see e.g. [1, 2]. Such damage parameters play a role of an "effective" load at a material point which correlates with the number of load cycles until crack initiation and substitutes the stress or strain range on the axis of ordinate in the conventional uniaxial stress-life or strain-life curve, respectively [11].

A particular goal of the analysis performed in this section is to examine whether certain fatigue damage parameter provides a consistent correlation with the fretting fatigue crack initiation for different specimen types and loading conditions and, hence, may be potentially considered in the fatigue assessment of full-scale axles. Among different damage parameters described in the literature, see e.g. [11], the following two quantities are considered below:

1) SWT parameter, P_{SWT}, according to Smith et al. [12] which includes effects due to both the principal strain range, $\Delta\varepsilon_1$, and the maximum normal stress, $\sigma_{n,max}$, acting in a particular plane:

$$P_{SWT} = \sqrt{\sigma_{n,max} \frac{\Delta\varepsilon_1}{2} E} \tag{1}$$

where E is Young's modulus.

2) Parameter P_{FS} according to Fatemi and Socie [13] which assumes that damage in a particular plane is promoted by the shear strain range, $\Delta\gamma$, and the related maximum normal stress, $\sigma_{n,max}$:

$$P_{FS} = \frac{\Delta\gamma}{2}\left(1 + k\,\frac{\sigma_{n,max}}{\sigma_0}\right) \tag{2}$$

The parameter k is a measure of the interaction between the shear and normal failure modes and can be determined by fitting specific test data. In this study, it was assumed that $k = 0.3$ and $\sigma_0 = 450$ MPa, representing the cyclic yield stress of the material EA4T.

The above fatigue parameters, P_{SWT} and P_{FS}, are applied along with the critical plane approach. The latter implies that the respective parameter is calculated at each material point for various plane orientations, while the maximum of the so determined values represents the measure of fatigue damage.

Fig. 15 shows the variation of the parameters P_{SWT} and P_{FS} versus the applied tensile stress σ_{appl} at different levels of the contact force. The curve oscillation (non-smooth behaviour) likely results from non-linearity of the numerical solution, in particular due to the fact that the position of the element with the highest parameter value changes in a discrete manner with changing external loads.

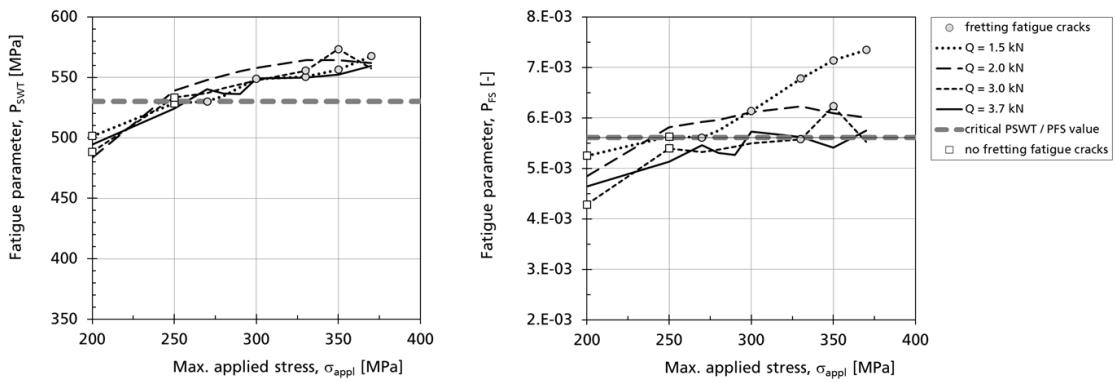

Fig. 15: Fatigue damage parameter P_{SWT} and P_{FS} as a function of σ_{appl}, at different levels of the transverse load, specimen #1.

An explanation for non-monotonic behaviour of the fatigue damage parameters is provided in Fig. 16 which shows stress-strain loops in the highly loaded element for the case of $Q = 3\ kN$ and $\sigma_{appl} =$

330, 350 and 370 MPa. The respective elements are numbered as 1, 2 and 3 in Fig. 10. Accordingly, the largest area of the stress-strain hysteresis is achieved at $\sigma_{appl} = 350$ MPa, thus corresponding with the local curve maximum in Fig. 15.

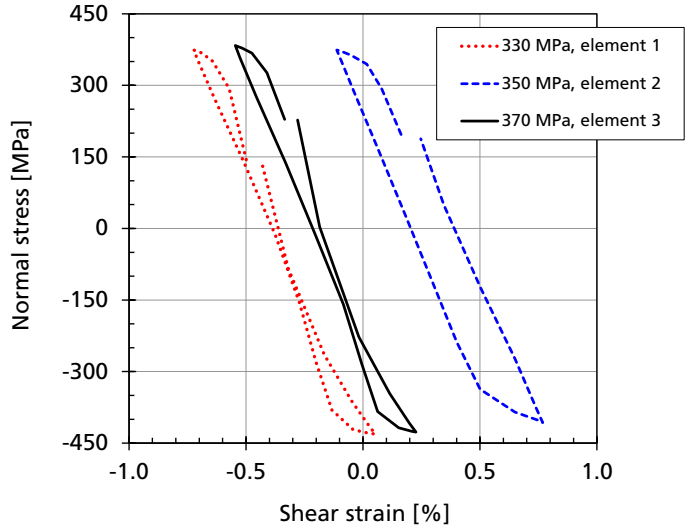

Fig. 16: Stress-strain variations in a load cycle for the highly loaded element. Example for $Q = 3$ kN and $\sigma_{appl} = 330, 350$ and 370 MPa.

3.3 Fretting Fatigue Assessment

In Fig. 15, the parameters P_{SWT} and P_{FS} are given as functions of the maximum applied stress σ_{appl} for different values of the transverse load Q. Test conditions leading to fretting fatigue crack initiation are marked by the circular symbols, whereas the square symbols indicate conditions under which no cracks were produced. The horizontal dashed lines give an estimate for the critical value of the respective fatigue parameters. Although both diagrams in Fig. 15 seem to provide a consistent description of the test results, the parameter P_{FS} is considered to be more appropriate as it takes into account the shear strain range $\Delta\gamma$ which is an essential deformation mode under fretting fatigue conditions. Moreover, P_{FS} is more sensitive to alterations of the loading conditions. Consequently, a critical value of $P_{FS} = 0.0056$ can be estimated, above which fretting fatigue cracks are achieved in the tests performed in this study.

Fig. 17 compares the fatigue damage parameter P_{FS} numerically estimated for different values of the contact length l_c. Accordingly, P_{FS} increases with increasing contact length. Note that the value of

$l_c = 1$ mm was only considered in the numerical analyses, whereas the final tests were performed using pads with the contact length $l_c = 1.7$ mm. The latter was estimated based on the results in Fig. 17, thus providing test conditions appropriate for the initiation of fretting fatigue cracks. At the same time, low P_{FS} values for round pads with an estimated contact length of $l_C = 0.2$ mm suggest that no initiation of fretting fatigue cracks is expected in the respective test series. These evaluation resultss are in accordance with the experimental findings, see Section 2.

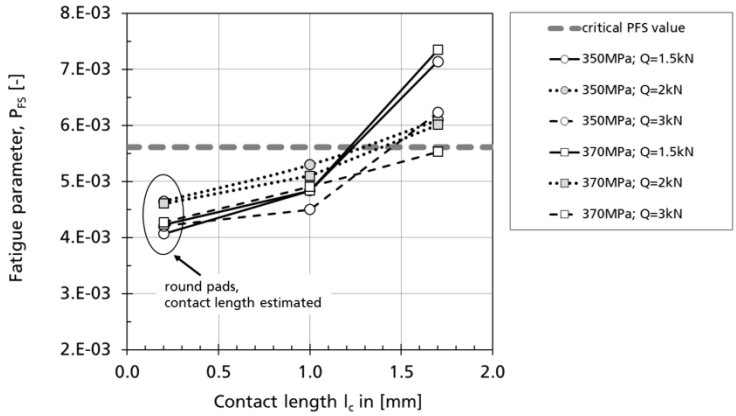

Fig. 17: Fatigue parameter P_{FS} as a function of the nominal (flattened pads) or estimated (round pads) contact length l_c.

Fig. 18 shows the influence of the uniform specimen length l_s on the fatigue parameters at a constant transverse load of $Q = 1.5$ kN. When comparing Fig. 13c and Fig. 14, the contact slip was concluded to increase with increasing l_s. As a consequence, the fatigue parameters increase with increasing slip, so that fretting fatigue cracks are achieved in the longer specimen at lower values of σ_{appl}. This behaviour is confirmed by the experimental data.

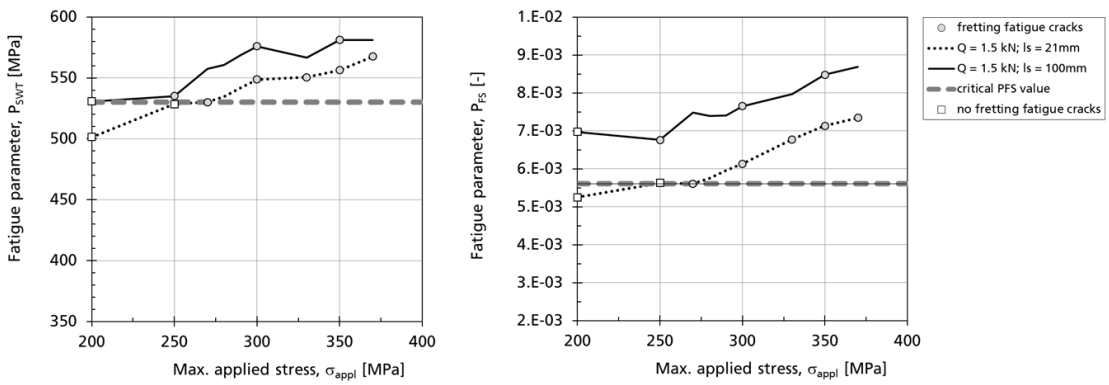

Fig. 18: Comparison of fatigue parameter P_{SWT} and P_{FS} for specimen #1 and specimen #2.

4. Summary and Conclusions

A fretting fatigue test set-up was developed which allows for a flexible variation of external loads (normal tension stress, transvers contact load) by which means reproducible series of fretting fatigue tests were successfully performed.

Experimental results demonstrate that increasing the contact area (change from a line to a surface contact) facilitates fretting fatigue crack initiation. Moreover, tests on specimens with different length revealed that the larger the contact slip the higher is the probability of crack initiation at the same nominal external load. For instance, when increasing the specimen uniform length from 21 mm to 100 mm, the tension stress required for fretting fatigue crack initiation reduces from $\sigma_{appl} = 270$ MPa to 250 MPa, while applying the same transverse load of $Q = 1.5$ kN.

A quantitative assessment of crack initiation under fretting fatigue conditions seems to be possible using fatigue damage parameters which take into account both the multiaxial stress state and non-proportional variation of the stress and strain fields within the contact area. Among two fatigue parameters applied within this study, P_{SWT} and P_{FS}, the latter (according to Fatemi and Socie [13]) is considered to be more appropriate for fretting fatigue conditions, as it explicitly takes into account the shear deformation mode within the contact zone. A critical value of the respective parameter leading to fretting fatigue crack initiation for the specimen and pad materials investigated (EA4T and ER8, respectively) was estimated to be $P_{FS} = 0.0056$. Using this value and based on results of numerical analyses, an optimal pad geometry with a flattened surface, $l_c = 1.7$ mm (Fig. 4b), was suggested leading to reproducible results in all subsequent tests.

Acknowledgements

This study was performed as a part of the cooperative research project EURAXLES funded by the European Commission within the 7th Framework Programme, Grant Agreement No 265706. This financial support as well as the cooperation with all project partners is gratefully acknowledged.

References

[1] Lykins CD, Mall S, Jain V. An evaluation of parameters for predicting fretting fatigue crack initiation. Int J Fatigue 2002;22:703-716.

[2] Lykins CD, Mall S, Jain V. Combined experimental-numerical investigation of fretting fatigue crack initiation. Int J Fatigue 2001;23703-711.

[3] Ekberg A. Fretting fatigue of railway axles – a review of predictive methods and an outline of a finite element model. J Rail Rapid Transit 2004;218:299–316.

[4] Beretta S, Cerrini A, Faustini V. A short crack model for fatigue limit of press-fittings in railway axles. In: 17th Nat. Conf. Italian Group of Fracture, Bologna, June 16-18; 2004.

[5] Varfolomeev I, Luke M, Burdack M. Fatigue and fretting fatigue behaviour of a railway axles steel A4T. In: 8th Int. Conf. on Contact Mechanics and Wear of Rail/Wheel Systems. Firenze, Italy, September 15-18; 2009.

[6] Makino T, Kato T, Hirakawa K. Review of the fatigue damage tolerance of high-speed railway axles in Japan. Engng Fract Mech 2011;78:810–825.

[7] ASTM E2789-10: Standard Guide for Fretting Fatigue Testing; 2010. DOI: 10.1520/E2789.

[8] Traupe M, Meinen H, Zenner H. Sichere und wirtschaftliche Auslegung von Eisenbahnfahrwerken (Safe and Economic Design of Running Gears). Final report, IMAB TU Clausthal; 2004.

[9] EURAXLES: Minimizing the risk of fatigue failure of railway axles. Collaborative project within the seventh framework programme, Grant Agreement No 265706. Full scale axle tests on Minden type axle test stand; 2014.

[10] Lemaitre J, Chaboche J-L. Mechanics of Solid Materials. Cambridge University Press; 1990.

[11] Socie DF, Marquis GB. Multiaxial Fatigue. SAE, Warrendale, PA; 2000.

[12] Smith RN, Watson P, Topper TH. A stress-strain parameter for the fatigue of metals. J. Materials 1970;5:767-778.

[13] Fatemi A, Socie DF. A critical plane approach to multiaxial fatigue damage including out of phase loading. Fatigue Fract. Eng. Mater. Struct. 1988;11:149-165.